Optimizing maximum carboxylation rate for North America's boreal forests in the Canadian Land Surface Scheme Including biogeochemical Cycles (CLASSIC) v.1.3

Author Responses

Dear Editors and Referees,

Please find herein all referee comments (in blue) along with our corresponding replies (in black) and our modifications to the manuscript (italicized in black).

Anonymous Referee #1

(**R1.C1**) This study utilized a Bayesian algorithm to optimize Vcmax25 in the land surface model against eddy covariance observations at eight mature boreal forest stands in North America. The results showed that the Bayesian algorithm can optimize Vcmax25 and improve ET and GPP estimates. The topic is interesting, and the results look promising. However, I am not convinced that the manuscript is innovative enough to contribute to the development of physical models, and therefore, I cannot accept it for publication.

Thank you for your time and efforts in reviewing our manuscript and providing constructive comments. We were pleased to read that you found the topic interesting and the results promising. In summary, we used a Bayesian optimization framework to optimize maximum carboxylation rate at 25 °C (V_{cmax25}) for representative plant functional types (PFTs) in North America's boreal forests in the Canadian Land Surface Scheme Including biogeochemical Cycles (CLASSIC, version 1.3) with observed daily carbon dioxide (CO_2) (i.e., gross primary productivity [GPP]) and water fluxes (i.e., evapotranspiration [ET]) obtained from eddy covariance measurements. To the best of our knowledge, this is a first study focusing on the Bayesian parameter optimization of V_{cmax} in boreal forest stands experiencing different climate and permafrost conditions with CLASSIC or other terrestrial biosphere models (TBMs) of similar complexity, e.g., CLM5 (Lawrence et al., 2019), LM4 (Dunne et al., 2020), and JULES3 (Slevin et al., 2017). Given that V_{cmax} is one of the most important parameters in many TBMs (Rogers, 2014), our optimizations with CLASSIC are highly relevant to other TBMs of similar

complexity. Therefore, we believe that our work represents an important step in improving the parameterization of V_{cmax} in TBMs across the boreal biome in North America.

The novelties of our study include refining V_{cmax} at the PFT level (compared to stand level as in previous studies, e.g., Ueyama et al., 2016) for boreal forests in North America using a Bayesian optimization framework. Considering the vast extent of the boreal biome in North America, adequately parameterizing V_{cmax} was identified as a key challenge hindering progress in TBM development (Rogers et al., 2021; Stinziano et al., 2019; Rogers, 2014; Fisher et al., 2018). Based on our previous work (Qu et al., 2023), CLASSIC showed limited model skill in reproducing observed daily GPP and ET using its default V_{cmax25} parameterization for one tree PFT (i.e., "evergreen needleleaf tree" [ENT]) in boreal forest stands in North America. The simple assumption of a stand-level V_{cmax25} constant in space and time might be a major contributor to the limited model skill. In addition to tree PFTs, boreal forest canopies often comprise various plant species and associated PFTs in their understory (e.g., shrubs and herbs) and ground cover (e.g., mosses and lichens), respectively. Thus, refining PFT-level V_{cmax} parameterizations to account for understory and ground cover PFTs is important for modeling boreal forest function including GPP and ET. This is especially true in boreal forest stands in the permafrost zone characterized by low tree stem densities (Heijmans et al., 2004; Ikawa et al., 2015). Previous optimization studies conducted in boreal forest stands optimized stand-level V_{cmax} with multilayer canopies by assuming a single tree PFT, e.g., ENT (He et al., 2014; Mo et al., 2008; Ueyama et al., 2016). Our Bayesian optimizations with CLASSIC were performed for six PFTs, collectively representing eight boreal forest stands in North America.

Our optimized PFT-level V_{cmax25} estimates provide an improved understanding of how V_{cmax25} for different tree, shrub and herb PFTs may vary spatially across the boreal biome in North America. For example, our "single-site" optimizations revealed large variation in V_{cmax25} for shrub and herb PFTs in forest stands. Additional analyses using a random forest regression approach showed that known predictors of GPP and ET including metrics of growing season timing (i.e., the start, end, and length of the growing season) and meteorological variables well explained the spatial variation in PFT-level V_{cmax25} (e.g., the end of the growing season for shrub PFTs). In addition, we collated V_{cmax25} estimates reported in the literature derived from in-situ leaf-level gas exchange measurements to support our analyses and discuss our findings.

In addition, GPP and ET simulated with CLASIC using the optimized PFT-level V_{cmax25} were compared with corresponding stand-level estimates derived from several gridded global data products that were produced using different observations (e.g., remote sensing data) and different process-based and statistical modeling approaches (Table 1 in the manuscript). The comparisons showed that CLASSIC GPP and ET were in better agreement with corresponding stand-level estimates when the optimized PFT-level V_{cmax25} was used instead of the default V_{cmax25} parameterization.

So far, our optimized PFT-level V_{cmax25} has been successfully applied in two TBM modeling studies with CLASSIC. The "all-sites" optimized V_{cmax25} for ENT was used to improve model performance at a regional scale in Arctic-boreal regions (Curasi et al., 2023). In addition, the optimized PFT-level V_{cmax25} is currently being used for developing a plant hydraulics parameterization in CLASSIC (Umair et al., 2023, in preparation). We believe that our study will inspire both TBM modeling and measurement communities to advance model development (e.g., GPP and ET simulations) and field measurements (e.g., photosynthetic capacity and V_{cmax}) in Arctic-boreal regions, respectively. Therefore, we believe that the topic of our manuscript is timely and warrants publication in *Geoscientific Model Development*.

We have carefully revised our manuscript to better clarify our motivation and the results of our study. New text is indicated in italics.

Section Abstract (Pages 1–2, Lines 19–38)

"The maximum carboxylation rate (V_{cmax}) is an important parameter for the coupled simulations of gross primary production (GPP) and evapotranspiration (ET) in terrestrial biosphere models (TBMs) such as the Canadian Land Surface Scheme Including biogeochemical Cycles (CLASSIC). *In-situ measurements of V_{cmax} show its spatio-temporal variation across the boreal biome in North America.* However, V_{cmax} in TBMs is often prescribed as constant in time and space for plant functional types (PFTs). *To reduce the uncertainty introduced by a spatially constant V_{cmax},* we used a Bayesian algorithm to optimize V_{cmax25} (V_{cmax} at 25 °C) in CLASSIC against *daily GPP and ET observations obtained from eddy covariance measurements* made over eight mature boreal forest stands in North America for six representative PFTs (two trees, two shrubs, and two herbs). Simulated GPP and ET with CLASSIC using the optimized PFT-level V_{cmax25} generally resulted in reduced root mean square deviation values compared with

corresponding stand-level estimates derived from several gridded global data products. The optimized PFT-level V_{cmax25} compared reasonably well with reported estimates in the literature derived from in-situ leaf-level gas exchange measurements. However, *we identified large spatial variation in the optimized PFT-level V_{cmax25} in forest stands, especially for shrub and "sedge" PFTs. We found that several meteorological variables and metrics of growing season timing (e.g., end of the growing season for shrub PFTs)* explained much of the spatial variation in the optimized PFT-level V_{cmax25}, providing a basis to improve V_{cmax} parameterization in TBMs at a regional scale *across the boreal biome in North America*."

Section 1 Introduction, Paragraphs 2–5 (Pages 2–4, Lines 52–102):

"The "Farquhar" model and its variants are commonly used in TBMs including CLASSIC to simulate gross primary production (GPP), i.e., photosynthetic CO_2 uptake, and evapotranspiration (ET) with coupled stomatal conductance–photosynthesis models (Farquhar et al., 1980; Leuning, 1995). The maximum carboxylation rate, V_{cmax}, is one of the most important parameters in the "Farquhar" model (Rogers, 2014). *Adequately parameterizing V_{cmax} has been widely identified as a key challenge hindering TBM development across the boreal biome (Rogers et al., 2021; Stinziano et al., 2019; Rogers, 2014; Fisher et al., 2018). Part of this challenge is due to the high sensitivity of V_{cmax} to plant traits and environmental conditions (Ali et al., 2015; Smith et al., 2019).* Foliar nutrients invested in photosynthetic proteins, particularly in the RuBisCO enzyme, determine V_{cmax} (Evans and Seemann, 1989). Through their influences on foliar nutrients, morphology, and nutrient use efficiency of photosynthesis (Musavi et al., 2016; Maire et al., 2015; Dong et al., 2020), environmental variables, e.g., air temperature, solar radiation, and atmospheric humidity, have been found to exert strong controls on V_{cmax} (Ali et al., 2015; Yan et al., 2023). The boreal biome is characterized by a short growing season, a low rate of soil mineralization, and thus limited soil nutrient availability, especially in the permafrost zone (Price et al., 2013). Plant phenology, closely associated with soil freeze-thaw and nutrient cycling processes (Rayment et al., 2002) and the seasonality of foliar ontogeny and chlorophyll content (Croft et al., 2017; Detto and Xu, 2020), may thus be important to V_{cmax} for boreal plant species. *However, comprehensive syntheses of in-situ V_{cmax} measurements that consistently examine and quantify spatio-temporal variation in V_{cmax} are currently lacking for boreal plant species, leading to an incomplete understanding of V_{cmax} across the boreal biome (Rogers et al., 2017).*

In general, the V_{cmax} parameterization in TBMs is often oversimplified, assuming that V_{cmax} is constant in time and space for plant functional types (PFTs). Based on an evaluation against eddy covariance observations, CLASSIC with its default V_{cmax25} (V_{cmax} at 25 °C) parameterization for one tree PFT (i.e., "evergreen needleleaf tree" [ENT]) showed limited model skill in reproducing observed daily GPP and ET in boreal forest stands in North America (Qu et al., 2023). The V_{cmax25} parameterization of constant values in space for PFTs might be a major contributor to the limited model skill. In addition to trees, boreal forest canopies often have various plant species and associated PFTs in their understory (e.g., shrubs and herbs) and ground cover (e.g., mosses and lichens), respectively. The understory and ground cover PFTs constitute non-negligible contributions to stand-level CO_2 and water fluxes in boreal forest stands (Gaumont-Guay et al., 2014). Thus, refining PFT-level V_{cmax} parameterizations to account for understory and ground cover PFTs is important for modeling boreal forest CO_2 and water fluxes, especially in the permafrost zone where boreal forest stands are generally characterized by low tree stem densities (Heijmans et al., 2004; Ikawa et al., 2015).

Eddy covariance measurements of CO_2 and water fluxes provide valuable data for TBM refinement and development (Schwalm et al., 2010; Bonan et al., 2011). Optimizing V_{cmax} in TBMs using eddy covariance observations for boreal forest stands has been the focus of several previous studies (He et al., 2014; Mo et al., 2008; Ueyama et al., 2016). *However, these optimizations were performed only on a single tree PFT, e.g., ENT by Ueyama et al. (2016), for boreal forest stands with multi-layer canopies and thus provided stand-level rather than PFT-level estimates of V_{cmax}.* In this study, we optimized V_{cmax25} in CLASSIC using daily GPP and ET simulations and daily observations obtained from eddy covariance measurements made over eight black spruce (*Picea mariana*)-dominated, mature boreal forest stands (>70 years old) in North America. *The optimizations were conducted at the PFT level for six representative PFTs (two trees, two shrubs, and two herbs) both in individual forest stands and across all forest stands.* Simulated daily GPP and ET with CLASSIC using the optimized PFT-level V_{cmax25} were compared with corresponding stand-level estimates derived from several gridded global data products. We compared the optimized PFT-level V_{cmax25} with estimates derived from in-situ leaf-level gas exchange measurements reported in the literature. *The spatial variation in the optimized PFT-level V_{cmax25} in forest stands was examined in relation to growing season timing and several meteorological variables using a random forest regression approach.*"

(**R1.C2**) 1) Data assimilation methods have been widely employed in the optimization of Vcmax25 (He et al., 2019). Data assimilation methods can improve the estimation of vegetation photosynthesis by assimilating remote sensing SIF data at regional or global scales. Although the results of this manuscript are reliable, I do not believe that site-level optimization can be extrapolated to regional or global scales. The expansion from site-specific to regional scales is crucial for the development of physical models.

Yes, we agree with the reviewer that extrapolating site-specific model parameters to regional or global scales is crucial for model development. Our study contributes to such efforts by using a model benchmarking dataset for boreal forest stands that are representative of major vegetation types (e.g., high and relatively low tree stem densities) and environmental gradients (e.g., climate and permafrost extent) across the boreal biome in North America (Qu et al., 2023). The resulting optimized PFT-level V_{cmax25} was used in this study to examine relationships between V_{cmax25} and a suite of known predictors using a random forest regression approach (Section 2.5 in the manuscript). Our findings will provide guidance for regional PFT-level V_{cmax} parameterizations across the boreal biome in North America.

We have revised our text to better convey these points.

Section 2.2, Paragraph 1 (Page 5, Lines 137–149):

"*Our optimizations used a model benchmarking dataset for boreal forests in North America (Fig.1 and Table S2) (Qu et al., 2023). The dataset integrates eddy covariance flux and supporting measurements (e.g., meteorology) made over eight mature boreal forest stands.* The overstory of forest stands are dominated by black spruce with tree canopy coverage ranging from 15 % to 90 %. Dominant understory vascular plants include dwarf shrubs, e.g., Labrador tea (*Rhododendron groenlandicum*), lingonberry (*Vaccinium vitis-idaea*), and blueberry (*Vaccinium spp.*), and sedges (e.g., *Carex spp.*). *The forest stands are distributed across East-West and South-North gradients in climate and permafrost extent across the boreal biome in North America. The model benchmarking dataset includes harmonized data of soils, permafrost, and plants, and gap-filled meteorological variables essential for stand-level parameterizations and simulations in TBMs. The CO_2 and water fluxes in the dataset were screened based on half-hourly data quality flags to obtain high quality daily aggregates.*"

Section 3.4, Paragraph 1 (Page 16, Lines 356–361):

"*In addition, our identified relationships between the optimized V_{cmax25} for ENT and the selected predictors will provide guidance for regional PFT-level V_{cmax} parameterizations across the boreal biome (Ali et al., 2015; Alton, 2017; Verheijen et al., 2013; Bauerle et al., 2012).* For example, incorporating a V_{cmax25}-TA or V_{cmax25}-SOS relationship could improve V_{cmax25} parametrization for ENT (Table 2) (Wullschleger et al., 2014; Verheijen et al., 2013)."

In addition, our Bayesian optimizations on PFT-level V_{cmax25} were designed to distinguish among contributions of different PFTs to stand-level GPP and ET in forest stands. We found that differences in the abundance of tree, shrub, and herb PFTs were important for explaining the spatial variation in V_{cmax25} in forest stands, e.g., tree PFTs with low optimized V_{cmax25} that were dominant in southern, permafrost-free forest stands compared with shrub and herb PFTs with relatively high V_{cmax25} that were more abundant in northern forest stands in the permafrost zone. This finding aligns well with stand-level V_{cmax25} estimates obtained from satellite chlorophyll fluorescence measurements across the boreal biome in North America by He et al. (2019) (please see their map in Fig. 2[a]).

We have added a statement to clarify this point.

Section 3.3, Paragraph 4 (Page 15, Lines 330–336):

"*Our results suggest that differences in the abundance of tree, shrub and herb PFTs could be important for explaining the spatial variation in the optimized V_{cmax25} in forest stands.* For example, ENT with low optimized V_{cmax25} was dominant in southern, permafrost-free forest stands while shrub and herb PFTs with relatively high optimized V_{cmax25} were more abundant in northern forest stands in the permafrost zone. *This finding is consistent with stand-level V_{cmax25} estimates obtained from satellite-based chlorophyll fluorescence measurements over the boreal biome in North America (He et al., 2019).*"

(**R1.C3**) 2) The authors need to provide more details about the model, including meteorological data and auxiliary data. Additionally, what is the timescale of Vcmax25 optimization? Is it on a daily, monthly, or throughout the entire growing season? Which years' observational data were used for optimizing Vcmax25? And which years' observational data were used for the spin-up? The site name, vegetation type, and other key information should be listed in the manuscript.

Thank you for pointing out these missing details. The manuscript has been revised accordingly. Please see our detailed responses below.

- The authors need to provide more details about the model, including meteorological data and auxiliary data.
- The site name, vegetation type, and other key information should be listed in the manuscript.

We have revised our statements in the Section 2.2 to explain the model benchmarking dataset used in this study (please see our responses to **R1.C2**). In addition, we have revised Table S2 with additional details on site characteristics and the dataset.

Supplementary materials, Table S2:

Table S2. Boreal forest stands in this study. Vegetation type refers to AmeriFlux vegetation classifications: evergreen needleleaf forests (ENF). Climate is the 30-year climate normals of average annual air temperature and average annual total precipitation. CLASSIC plant functional types (PFTs) are "evergreen needleleaf tree" (ENT), "deciduous needleleaf tree" (DNT), "evergreen broadleaf shrub" (EBS), "deciduous broadleaf shrub" (DBS), "C3 grass" (C3G), and "sedge" (SDG). Soils are the permeable depth (PD), near-surface organic layer thickness (OLT), and soil texture including sand (S), clay (C), silt (Si), sandy loam (SL), silt loam (SiL), silty clay loam (SiCL), and silty clay (SiC). Permafrost is isolated (≤10 % in areal extent), sporadic (>10–50 %), discontinuous (>50–90 %), and continuous (>90 %). Forest stand names refer to AmeriFlux IDs: CA-Qfo (Quebec—Eastern Boreal, Mature Black Spruce), CA-Obs (Saskatchewan—Western Boreal, Mature Black Spruce [in the former BOREAS Southern Study Area]), CA-Man (Manitoba—Northern Old Black Spruce [in the former BOREAS Northern Study Area]), CA-SMC (Smith Creek), US-BZS (Bonanza Creek Black Spruce), US-Uaf (University of Alaska, Fairbanks), US-Prr (Poker Flat Research Range Black Spruce Forest), and CA-HPC (Havikpak Creek). Forest stands are in a latitudinal order from south (CA-Qfo) to north (CA-HPC) (Fig. 1).

Name (AmeriFlux ID)	*Vegetation type*	*Location*	*Climate*	*PFTs*	*Soils*	*Permafrost*	*Period*	*Reference*
CA-Qfo	*ENF*	*49.69, -74.34*	*0.2 ℃, 929 mm*	*90 % ENT, 10 % DBS*	*31 m PD, 30 cm OLT, SL*	*Absent*	*2003–2010*	*Bergeron et al. (2007)*
CA-Obs	*ENF*	*53.99, -105.12*	*1.1 ℃, 474 mm*	*90 % ENT, 10 % DNT*	*32 m PD, 30 cm OLT, SL/S*	*Absent*	*1997–2010*	*Krishnan et al. (2008)*
CA-Man	*ENF*	*55.88, -98.48*	*-1.7 ℃, 324 mm*	*90 % ENT, 5 % EBS, 5 % DBS*	*36 m PD, 40 cm OLT, C*	*Absent*	*1994–2008*	*Dunn et al. (2007)*
CA-SMC	*ENF*	*63.15, -123.25*	*-2.8 ℃, 389 mm*	*22 % ENT, 34 % EBS, 12 % DBS, 15 % SDG*	*46 m PD, 130 cm OLT, SiC/SiCL*	*Discontinuous*	*2017–2018*	*Helbig et al. (2017)*
US-BZS	*ENF*	*64.7, -148.32*	*-2.0 ℃, 280 mm*	*21 % ENT, 43 % EBS, 13 % DBS, 23 % SDG*	*16 m PD, 100 cm OLT, Si*	*Discontinuous*	*2014–2018*	*Euskirchen et al. (2014)*
US-Uaf	*ENF*	*64.87, -147.86*	*-3.9 ℃, 367 mm*	*20 % ENT, 45 % EBS, 10 % DBS, 25 % SDG*	*16 m PD, 60 cm OLT, SiL*	*Discontinuous*	*2003–2018*	*Ueyama et al. (2014)*
US-Prr	*ENF*	*65.12, -147.49*	*-2.9 ℃, 391 mm*	*20 % ENT, 14 % EBS, 13 % DBS, 24 % SDG*	*5 m PD, 40 cm OLT, SiL*	*Discontinuous*	*2010–2014*	*Ikawa et al. (2015)*
CA-HPC	*ENF*	*68.32, -133.52*	*-6.8 ℃, 235 mm*	*15 % ENT, 58 % EBS, 5 % DBS, 4 % C3G*	*7 m PD, 50 cm OLT, SiC*	*Continuous*	*2016–2018*	*Martin et al. (2022)*

- Additionally, what is the timescale of Vcmax25 optimization? Is it on a daily, monthly, or throughout the entire growing season?

Our optimizations were performed at the daily time scale using daily GPP and ET simulated with CLASSIC and daily observations of GPP and ET obtained from eddy covariance measurements. We have revised our statements to clarify this point.

Section 2.3, Paragraph 1 (Page 6, Lines 161–165):

"*To well constrain PFT-level V_{cmax25} in CLASSIC, we defined cost function based on GPP and ET (Groenendijk et al., 2011a; Ueyama et al., 2016; He et al., 2014)*. Specifically, the cost function was the normalized root mean square error ($RMSE_n$) of *daily GPP (g C m^{-2} day^{-1}) and ET (mm day^{-1}) simulated with CLASSIC and corresponding daily observations obtained from eddy covariance measurements*."

Also, e.g., Section 1, Paragraph 5 (Page 3, Lines 92–94):

"In this study, we optimized V_{cmax25} in CLASSIC using *daily GPP and ET simulations and daily observations* obtained from eddy covariance measurements made over eight black spruce (*Picea mariana*)-dominated, mature boreal forest stands (>70 years old) in North America."

and Section 3.1, Paragraph 1 (Page 9, Lines 233–234):

"Model performance regarding *daily* GPP and ET improved in most forest stands (e.g., lower RMSD) using the "single-site" optimized PFT-level V_{cmax25} (Fig. 3a and b)."

- Which years' observational data were used for optimizing Vcmax25? And which years' observational data were used for the spin-up?

We have revised Table S2 showing the temporal coverage of the observations in the model benchmarking dataset used for the optimizations. The model spin-up procedure was performed using the gap-filled meteorological observations in the dataset. We have revised a statement to clarify the spin-up procedure.

Section 2.3, Paragraph 3 (Page 7, Lines 180–182):

"For each iteration, a spin-up procedure in CLASSIC was first performed *using the gap-filled meteorological observations in the dataset (Section 2.2)* to equilibrate model, defined by the simulated total carbon pool varying less than 0.1 % compared to the last loop (Qu et al., 2023)."

(**R1.C4**) 3) This study lacks independent validation. Eddy covariance observations of ET and GPP were used to optimize Vcmax25. Subsequently, the optimized Vcmax25 estimates of ET and GPP were further compared with eddy covariance observations. Although some global gridded products have been used to assess model simulation results, these gridded products exhibit uncertainty, and their observational footprints do not align with eddy covariance observations.

To ensure robust optimizations of PFT-level V_{cmax25} with good model performance at different time scales (i.e., daily, seasonal, and interannual), our optimizations used all available daily GPP and ET observations obtained from eddy covariance measurements made over forest stands similar to previous studies (Santaren et al., 2007; Druel et al., 2017; Kuppel et al., 2012). We have added a schematic diagram to explain the Bayesian optimization framework used for the optimizations (please see our responses to **R2.C2**). We did not perform an independent evaluation on the optimizations using GPP and ET observations obtained from eddy covariance measurements. Through two statistical metrics (i.e., root mean square deviation and Pearson correlation coefficient) that are different from the cost function of the optimizations, we evaluated GPP and ET simulated with CLASSIC using the optimized PFT-level V_{cmax25} against the observations of GPP and ET used for the optimizations. These comparisons provided first-order insights into whether the optimizations actually improved the model performance regarding daily GPP and ET.

We have revised our statements to clarify our points. In addition, please see our responses to **R2.C7** for an additional evaluation of model performance using the optimized PFT-level V_{cmax25} at the daily time scale.

Section 2.5, Paragraph 1 (Page 9, Lines 209–213):

"*To examine whether the optimizations improved model performance, we used the root mean square deviation (RMSD) and Pearson correlation coefficient (r) to evaluate the performance of simulated daily GPP and ET with CLASSIC using the optimized PFT-level V_{cmax25} against the same observations also used for the optimizations (Kuppel et al., 2012).*"

Section 3.1, Paragraph 1 (Pages 9–10, Lines 233–244):

"Model performance regarding daily GPP and ET improved in most forest stands (e.g., lower RMSD) using the "single-site" optimized PFT-level V_{cmax25} (Fig. 3a and b). *Exceptions include GPP at US-Uaf and ET at US-BZS and US-Prr as indicated by slightly increased RMSD. Model performance improvement using the "single-site" optimized PFT-level V_{cmax25} was also found in the observed seasonality of daily GPP and ET in all forest stands (Fig. S3 and S4). Simulated daily GPP and ET using the "single-site" optimized PFT-level V_{cmax25} were significantly correlated with observed daily GPP (r = 0.79 to 0.94) and ET (r = 0.81 to 0.92). In addition, enhanced correlations between daily GPP simulations using the "single-site" optimized PFT-*

level V_{cmax25} and observations were found in most forest stands (Table S4). Similar improvements of model performance were achieved with the "all-sites" optimization."

In addition, we used independent data of corresponding stand-level GPP and ET estimates derived from several gridded global data products for comparisons with CLASSIC simulations using the optimized PFT-level V_{cmax25}. Similar model-data comparisons using gridded global data products were used in previous modeling studies at eddy covariance sites (Kuppel et al., 2014; Tramontana et al., 2016; Xiao et al., 2014; Ueyama et al., 2016; Groenendijk et al., 2011b; Friend et al., 2007). Please see our responses to **R1.C1** for further clarification.

(**R1.C5**) 4) In this study, the random forest method was employed to characterize the relative importance of various influencing factors on Vcmax25. The limited optimization of Vcmax25 values in this study may lead to overfitting or underfitting issues in the machine learning method. This will impact the credibility of the relative importance results.

He, L., Chen, J. M., Liu, J., Zheng, T., Wang, R., Joiner, J., Chou, S., Chen, B., Liu, Y., and Liu, R.: Diverse photosynthetic capacity of global ecosystems mapped by satellite chlorophyll fluorescence measurements, Remote Sens. Environ., 232, 111344, https://doi.org/10.1016/j.rse.2019.111344, 2019.

Random forests average the output of a large number of randomized decision trees to improve the predictive accuracy and thus are less susceptible to overfitting due to the Law of Large Numbers (Breiman, 2001). In this study, we used 1000 decision trees in each random forest to reduce overfitting. To address this comment, we have removed "latitude" as a predictor to increase the robustness of random forest regressions because of the strong covariance of "latitude" with other predictors (e.g., air temperature and solar radiation) that may lead to overfitting. In addition, the burn-in period of the optimizations has also been removed to avoid PFT-level V_{cmax25} estimates with relatively poor model performance of CLASSIC.

In addition, we have added a bootstrapping procedure to quantify the uncertainty in the relationships between the optimized PFT-level V_{cmax25} and the predictors resulting from uncertainty in the optimizations. Our revised results showed that R^2, the coefficient of determination, for the random forest regressions ranged from 0.79 ± 0.04 to 0.89 ± 0.05 among the PFTs, suggesting well-fitted random forest regressions.

Accordingly, we have revised the manuscript sections describing methodology, results, and discussion, respectively. New text is indicated in italics.

Section 2.3, Paragraph 3 (Page 7, Lines 185–190):

"The optimizations included a burn-in period during which the optimized PFT-level V_{cmax25} by TPE generally led to relatively poor CLASSIC performance (Fig. S1 and S2) (Gelbart et al., 2014). In this study, we treated the first 200 iterations as the burn-in period after which the convergence of optimizations was generally reached in this study (Sahlin, 2011). The burn-in period was removed in estimating posterior distributions of the optimized PFT-level V_{cmax25} (Nimalan et al., 2012)."

Section 2.5, Paragraph 1 (Page 9, Lines 213–230):

"A random forest regression approach was used to examine relationships between the "single-site" optimized PFT-level V_{cmax25} and a suite of predictors including metrics of growing season timing and several meteorological variables. *Specifically, meteorological variables included incoming shortwave radiation (SW), air temperature (TA), total precipitation (P), and vapor pressure deficit (VPD) (Ali et al., 2015; Yan et al., 2023). Metrics of growing season timing were the start (SOS), end (EOS), and length of the growing season (LOS), derived from observed daily GPP time series (Section 2.3). We calculated the multi-year averages of growing season timing (SOS [day of year], EOS [day of year], and LOS [days]), and the growing-season averages (SW [W m^{-2}], TA [°C], and VPD [hPa]) and sums (P [mm]) of meteorological variables. Random forests average the result of a large number of randomized decision trees to improve predictive accuracy and thus are less susceptible to overfitting due to the Law of Large Numbers (Breiman, 2001).* In each random forest we employed 1000 decision trees to reduce overfitting using the scikit-learn Python package (Pedregosa et al., 2011). The relative importance of the predictors was estimated using the impurity-based feature importance (Strobl et al., 2007). Partial dependence plots were produced to illustrate *relationships between the optimized PFT-level V_{cmax25} and the predictors (Goldstein et al., 2015; Baltzer et al., 2021). Additionally, a bootstrapping approach was used to quantify uncertainty in the relative importance of the predictors and the partial dependence due to the uncertainty in the optimizations (Schratz et al., 2019). Specifically, the optimized PFT-level V_{cmax25} in each forest stand was randomly resampled for random forest regressions with replacement 5000 times.*"

Section 3.3, Table 2:

Table 2. Model accuracy of random forest regressions (coefficient of determination, R^2) to predict plant functional type (PFT)-level V_{cmax25} and relative importance of predictors (Section 2.5). The metrics of growing season timing are the start (SOS, day of year), end (EOS, day of year), and length of the growing season (LOS, days). Meteorological variables are incoming shortwave radiation (SW, W m^{-2}), air temperature (TA, °C), total precipitation (P, mm), and vapor pressure deficit (VPD, hPa). CLASSIC PFTs are "evergreen needleleaf tree" (ENT), "evergreen broadleaf shrub" (EBS), "deciduous broadleaf shrub" (DBS), and "sedge" (SDG). *The standard deviation was estimated based on bootstrapping (Section 2.5). Partial dependence plots on predictors are shown in Fig. S5.*

PFT	*R^2*	*SOS*	*EOS*	*LOS*	*SW*	*TA*	*P*	*VPD*
ENT	*0.81 ± 0.04*	*0.31 ± 0.10*	*0.05 ± 0.04*	*0.08 ± 0.04*	*0.04 ± 0.08*	*0.34 ± 0.09*	*0.07 ± 0.04*	*0.12 ± 0.09*
EBS	*0.79 ± 0.04*	*0.20 ± 0.07*	*0.38 ± 0.09*	*0.09 ± 0.04*	*0.09 ± 0.09*	*0.05 ± 0.05*	*0.07 ± 0.04*	*0.12 ± 0.06*
DBS	*0.89 ± 0.05*	*0.15 ± 0.08*	*0.42 ± 0.10*	*0.12 ± 0.05*	*0.11 ± 0.08*	*0.05 ± 0.06*	*0.06 ± 0.03*	*0.09 ± 0.09*
SDG	*0.85 ± 0.03*	*0.10 ± 0.05*	*0.12 ± 0.04*	*0.13 ± 0.04*	*0.33 ± 0.06*	*0.10 ± 0.04*	*0.11 ± 0.04*	*0.11 ± 0.04*

Supplementary materials, Figure S5:

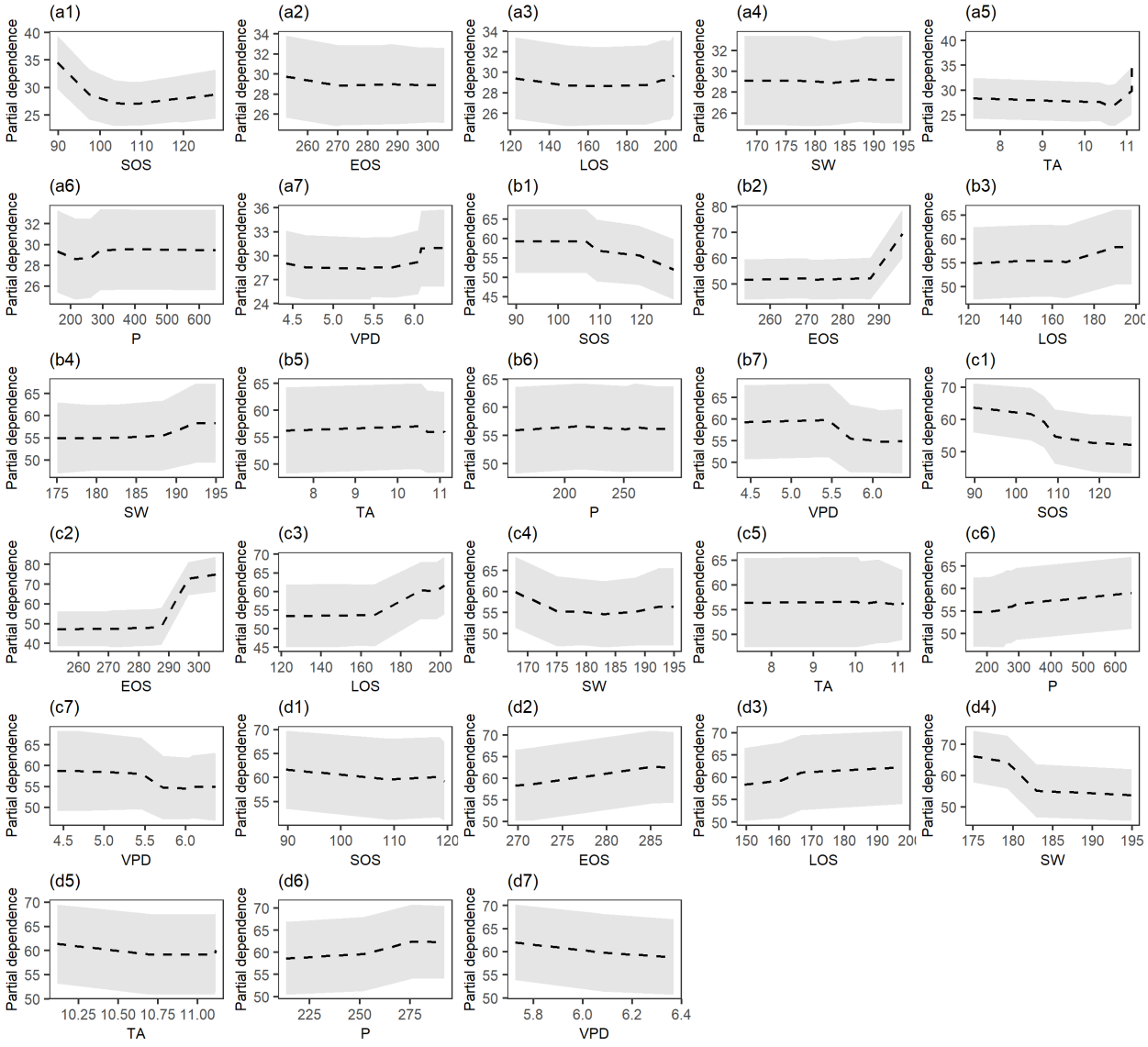

Figure S5. Partial dependence plots of random forest regression analyses for the optimized V_{cmax25} for CLASSIC plant functional types: "evergreen needleleaf tree" (a1–a7), "evergreen broadleaf shrub" (b1–b7), "deciduous broadleaf shrub" (c1–c7), and "sedge" (d1–d7). The metrics of growing season timing are the start (SOS, day of year), end (EOS, day of year), and length of the growing season (LOS, days). Meteorological variables are incoming shortwave radiation (SW, W m^{-2}), air temperature (TA, °C), total precipitation (P, mm), and vapor pressure deficit (VPD, hPa). The shaded area represents the bootstrapped standard deviation (Section 2.5).

Section 3.3, Paragraphs 1–3 (Pages 14–15, Lines 297–326):

"Random forest regressions suggested that the variation in the "single-site" optimized PFT-level V_{cmax25} in forest stands was well explained by the selected predictors (R^2 = 0.79 to 0.89, Table 2). The metrics of growing season timing, particularly SOS and EOS, were found to be important in explaining the variation for shrub PFTs and ENT. Partial dependence plots further showed that shrub PFTs and ENT tended to have high optimized V_{cmax25} in forest stands with an early SOS and/or late EOS (Fig. S5). A strong relationship between in-situ measured V_{cmax} and leaf nutrients (e.g., nitrogen) was widely found for various plant species over the globe (Kattge et al., 2009; Liang et al., 2020). In this study, the identified relationships between the optimized V_{cmax25} and growing season timing could be related to boreal forest soil temperature and moisture regimes (Cai and Dang, 2002; Reich et al., 2018). For example, SOS was found to be controlled by the timing of soil thaw in spring (Ahmed et al., 2021), which is important for soil microbial activities and nutrient cycling across the boreal biome (Salmon et al., 2016; Jasinski et al., 2022). In addition, an early SOS and/or late EOS generally correspond to a longer LOS, thus enhancing nutrient availability for boreal plant species and promoting relatively high V_{cmax25}, e.g., for shrub PFTs at CA-Qfo and CA-Man (Fig. 4a).

None of the selected meteorological variables could explain the variation in the optimized V_{cmax25} for shrub PFTs in forest stands. In contrast, important influences of TA and SW on the optimized V_{cmax25} were observed for ENT and SDG, respectively (Table 2). High TA may alleviate nutrient limitations on boreal plant species (Allison and Treseder, 2011), partially explaining the revealed positive influence of TA on the optimized V_{cmax25} for ENT (Fig. S5). The influence of SW on the optimized V_{cmax25} for SDG may be related to low-light environments for understory herbs in boreal forest stands (Tonteri et al., 2016). However, the uncertainty in the influence of SW for SDG may be relatively large due to the limited number of forest stands dominated by this PFT in this study (Fig. 4a)."

Additionally, because of the removal of the burn-in period in the optimizations, we have revised our results and discussion in Sections 3.1 and 3.2 accordingly.

Section 3.1, Figure 3:

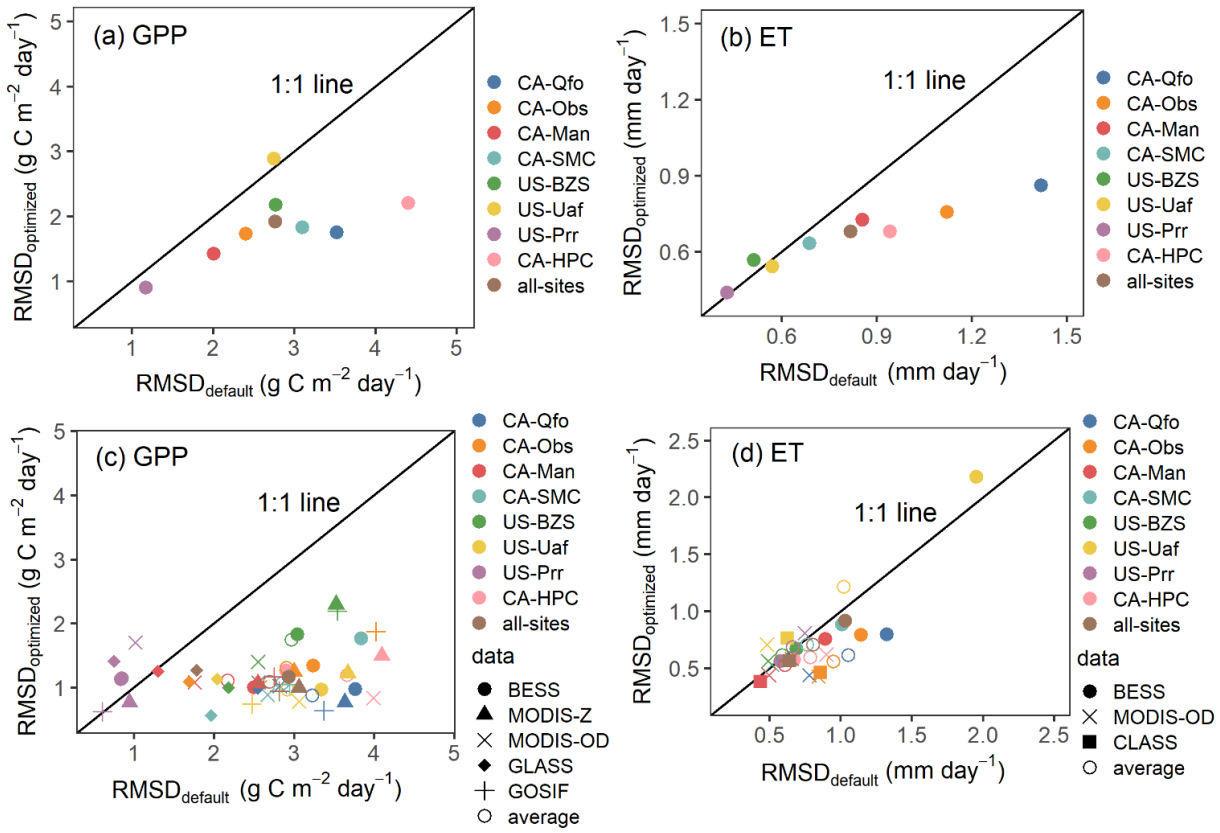

Figure 3. Root mean square deviation (RMSD) of CLASSIC gross primary production (GPP) and evapotranspiration (ET) using the default and optimized plant functional type-level V_{cmax25} ("single-site" and "all-sites") compared with observations obtained from eddy covariance measurements (a, b) and corresponding stand-level estimates (c, d). In panels (a) and (b), the same observations for the optimizations were used to examine whether the optimizations improved model performance regarding daily GPP and ET. The corresponding stand-level estimates were derived from gridded global data products of BESS (Li et al., 2021), MODIS-Z (Zhang et al., 2017), MODIS-OD (Running and Zhao, 2021), GLASS (Liang et al., 2021), GOSIF (Li and Xiao, 2019), and CLASS (Hobeichi et al., 2020) (Table 1). Forest stand names refer to AmeriFlux IDs and forest stands are ordered by latitude from south (CA-Qfo) to north (CA-HPC) (Fig. 1).

Section 3.2, Figure 4:

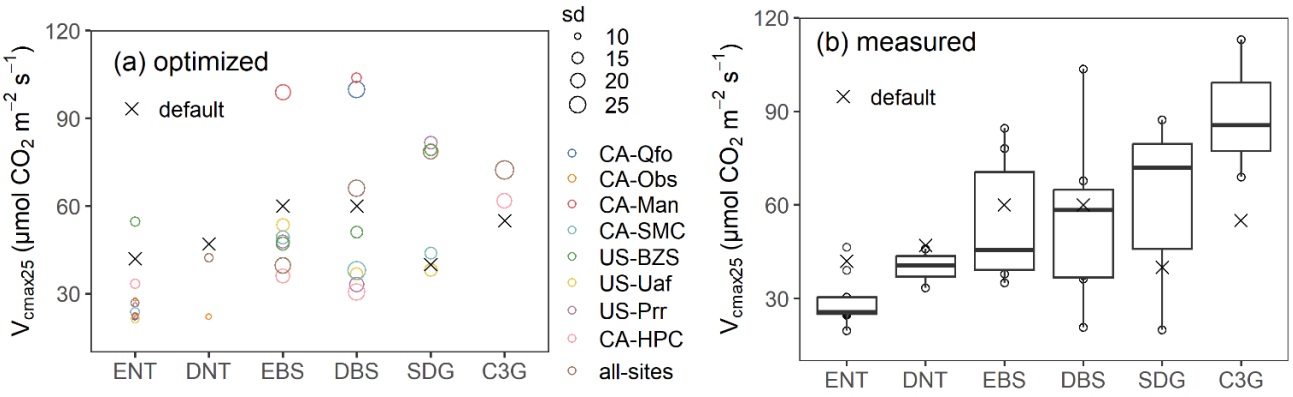

Figure 4. Plant functional type (PFT)-level V_{cmax25} from (a) "single-site" and "all-sites" optimizations and (b) estimates derived from leaf-level gas exchange measurements reported in the literature (Table S3) compared with the default V_{cmax25} values in CLASSIC. CLASSIC PFTs are "evergreen needleleaf tree" (ENT), "deciduous needleleaf tree" (DNT), "evergreen broadleaf shrub" (EBS), "deciduous broadleaf shrub" (DBS), "C3 grass" (C3G), and "sedge" (SDG). In panel (a), point sizes indicate the standard deviation (sd; μmol CO_2 m^{-2} s^{-1}) of the optimized PFT-level V_{cmax25} (Section 2.5). Forest stand names refer to AmeriFlux IDs and forest stands are ordered by latitude from south (CA-Qfo) to north (CA-HPC) (Fig. 1).

Supplementary materials, Table S4:

Table S4. CLASSIC model performance (average ± standard deviation) in root mean square deviation (RMSD) and Pearson correlation coefficient (r) using the default and optimized plant functional type (PFT)-level V_{cmax25} ("single-site" and "all-sites") compared with daily gross primary production (GPP) and evapotranspiration (ET) observations obtained from eddy covariance measurements made over forest stands. All Pearson correlation coefficients are statistically significant (α = 0.05). The units of RMSD are g C m^{-2} day^{-1} for GPP and mm day^{-1} for ET. Forest stand names refer to AmeriFlux IDs and forest stands are in a latitudinal order from south (CA-Qfo) to north (CA-HPC) (Fig. 1 and Table S2).

Flux	*Statistical metrics*	*PFT-level V_{cmax25}*	*CA-Qfo*	*CA-Obs*	*CA-Man*	*CA-SMC*	*US-BZS*	*US-Uaf*	*US-Prr*	*CA-HPC*
GPP	*RMSD*	*"single-site"*	*1.75 ± 1.13*	*1.73 ± 0.87*	*1.42 ± 0.51*	*1.82 ± 0.85*	*2.17 ± 1.54*	*2.89 ± 0.91*	*0.90 ± 0.30*	*2.21 ± 1.61*

		"all-sites"	*2.0 ± 1.3*	*1.9 ± 0.9*	*1.6 ± 0.7*	*2.1 ± 1.1*	*2.3 ± 1.1*	*2.9 ± 0.9*	*1.1 ± 0.4*	*2.6 ± 2.0*
		default	*3.52*	*2.40*	*2.00*	*3.10*	*2.77*	*2.74*	*1.17*	*4.40*
	r	*"single-site"*	*0.89 ± 0.01*	*0.89 ± 0.01*	*0.89 ± 0.04*	*0.79 ± 0.01*	*0.94 ± 0.0003*	*0.81 ± 0.03*	*0.91 ± 0.01*	*0.91 ± 0.01*
		"all-sites"	*0.89 ± 0.01*	*0.88 ± 0.02*	*0.89 ± 0.03*	*0.79 ± 0.01*	*0.93 ± 0.01*	*0.84 ± 0.02*	*0.90 ± 0.01*	*0.91 ± 0.01*
		default	*0.87*	*0.86*	*0.82*	*0.79*	*0.93*	*0.83*	*0.89*	*0.90*
ET	*RMSD*	*"single-site"*	*0.86 ± 0.27*	*0.76 ± 0.13*	*0.73 ± 0.07*	*0.63 ± 0.04*	*0.57 ± 0.10*	*0.54 ± 0.05*	*0.44 ± 0.03*	*0.68 ± 0.89*
		"all-sites"	*0.95 ± 0.29*	*0.80 ± 0.19*	*0.75 ± 0.08*	*0.70 ± 0.08*	*0.53 ± 0.08*	*0.59 ± 0.07*	*0.46 ± 0.03*	*0.76 ± 0.12*
		default	*1.42*	*1.12*	*0.85*	*0.69*	*0.51*	*0.57*	*0.43*	*0.94*
	r	*"single-site"*	*0.83 ± 0.01*	*0.81 ± 0.04*	*0.84 ± 0.01*	*0.87 ± 0.02*	*0.92 ± 0.01*	*0.87 ± 0.04*	*0.92 ± 0.01*	*0.83 ± 0.06*
		"all-sites"	*0.82 ± 0.01*	*0.85 ± 0.02*	*0.83 ± 0.02*	*0.88 ± 0.03*	*0.91 ± 0.01*	*0.86 ± 0.03*	*0.93 ± 0.02*	*0.84 ± 0.07*
		default	*0.78*	*0.84*	*0.84*	*0.90*	*0.91*	*0.90*	*0.92*	*0.88*

Supplementary materials, Table S5:

Table S5. Root mean square deviation (average ± standard deviation) averaged across all forest stands of CLASSIC simulations using the default and optimized plant functional type (PFT)-level V_{cmax25} ("single-site" and "all-sites") compared with the corresponding stand-level estimates of gross primary production (GPP) and evapotranspiration (ET). The corresponding stand-level estimates were derived from gridded global data products including BESS (Li et al., 2021), MODIS-Z (Zhang et al., 2017), MODIS-OD (Running and Zhao, 2021), GLASS (Liang et al., 2021), GOSIF (Li and Xiao, 2019), and CLASS (Hobeichi et al., 2020) (Table 1). The units are g C m^{-2} day^{-1} for GPP and mm day^{-1} for ET.

Flux	*PFT-level V_{cmax25}*	*BESS*	*MODIS-OD*	*MODIS-Z*	*GLASS*	*GOSIF*	*CLASS*	*Average*
GPP	*"single-site"*	*1.29*	*1.09*	*1.27*	*1.06*	*1.18*	*/*	*1.18*
	"all-sites"	*1.17*	*1.08*	*1.00*	*1.27*	*0.94*	*/*	*1.09*
	default	*2.93*	*2.56*	*3.06*	*1.78*	*2.82*	*/*	*2.63*
ET	*"single-site"*	*0.90*	*0.56*	*/*	*/*	*/*	*0.54*	*0.67*
	"all-sites"	*0.92*	*0.58*	*/*	*/*	*/*	*0.57*	*0.69*
	default	*1.03*	*0.66*	*/*	*/*	*/*	*0.64*	*0.78*

Also, e.g., Section 3.1, Paragraph 2 (Page 10, Lines 249–252):

"In contrast, a notable reduction in $RMSD_a$ of simulated ET using the "single-site" optimized PFT-level V_{cmax25} was found in two permafrost-free forest stands, CA-Qfo and CA-Obs, where $RMSD_a$ was reduced by *approximately 41 %* in each forest stand (Fig. 3d)."

Anonymous Referee #2

(**R2.C1**) Vcmax is an important parameter for TBMs. Simply setting Vcmax25 in TBMS induces the uncertainty of TBMs. In this paper, authors conducted a Bayesian algorithm to optimize Vcmax25 in CLASSIC against eddy covariance observations at eight mature boreal forest stands in North America for six representative PFTs and identified the spatial variability of Vcmax25. This paper try to explore the Vcmax change in boreal forests. However, l am major concerned about optimizing strategy used in this study.

We thank you for your time and efforts in reviewing our manuscript and providing constructive comments that have helped to improve it.

(**R2.C2**) 1. How to use TPE to optimize Vcmax25 was not explained in section 2.3. Vcmax was optimized in what time scale, yearly or daily? And in single-site optimization, for example, the observations were only the GPP and ET of the whole site. Does this result in ill-fitting problems when optimizing Vcmax for multiple PFTs simultaneously?

Please see our detailed responses below; the manuscript has been revised accordingly.

- How to use TPE to optimize Vcmax25 was not explained in section 2.3.

To address this comment, we have added a schematic diagram and revised our statements to explain how the tree-structured Parzen estimator (TPE) was used in the optimizations.

Section 2.3, Paragraph 3 (Page 7, Lines 176–179):

"The TPE algorithm iteratively minimized the cost function based on the Bayes' rule of conditional probability (Fig. 2) (Ellison, 2004; Bergstra et al., 2011). In each iteration, it optimized the expected improvement to predict a promising configuration of PFT-level V_{cmax25} *(Text S1)."*

Section 2.3, Figure 2:

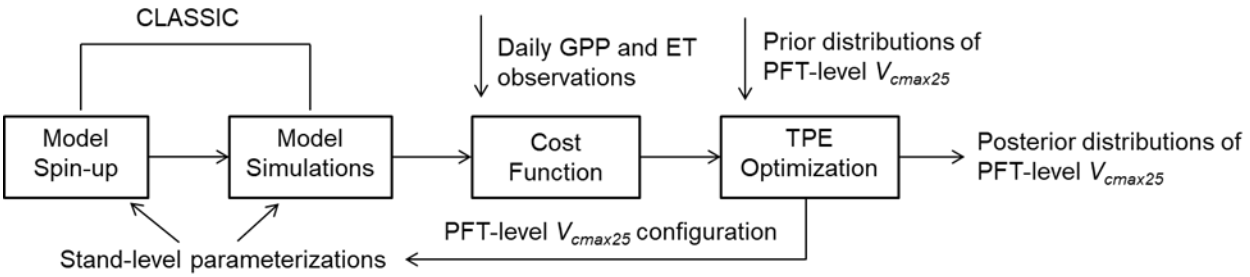

Figure 2. Bayesian optimization framework based on the tree-structured Parzen estimator (TPE) to optimize plant functional type (PFT)-level V_{cmax25} in CLASSIC against observed daily gross primary production (GPP) and evapotranspiration (ET) obtained from eddy covariance measurements.

Supplementary materials, Text S1:

"*The TPE optimization is performed based on the expected improvement (EI):*

$$EI(v) = \frac{qf'l(v) - l(v)\int_{-\infty}^{f'} p(f(v))df}{ql(v) + (1-q)g(v)}, \quad (S1)$$

defined by cost function $f(v)$ (i.e., the normalized root mean square error in Eq. 5) and its two probability densities $l(v)$ and $g(v)$. $f(v)$ is the set of $f(v_i)$ corresponding to a parameter configuration (v_i, i.e., V_{cmax} for plant functional types [PFTs]) optimized by the TPE algorithm. $l(v)$ is the probability density of $f(v_i)$ when $f(v_i) < f'$ and $g(v)$ is the density of the remaining $f(v_i)$. f' is a quantile value q so that $p(f(v) < f') = q$, set to 0.15 following Bergstra et al. (2015)."

- Vcmax was optimized in what time scale, yearly or daily?

Our optimizations were performed in the daily time scale. We have revised our statements to clarify this point. Please see our responses to **R1.C3**.

- And in single-site optimization, for example, the observations were only the GPP and ET of the whole site. Does this result in ill-fitting problems when optimizing Vcmax for multiple PFTs simultaneously?

Our "single-site" optimizations used all available daily GPP and ET observations as the constraints to ensure robust optimizations of PFT-level V_{cmax25} with good model performance in

different time scales (i.e., daily, seasonal, and interannual). The constraints resulted in well-fitted TPE optimizations and well-constrained PFT-level V_{cmax25} in forest stands (please see the optimized PFT-level V_{cmax25} in Figure 4a in the response to **R1.C5**). To provide first-order insights into the performance improvement of CLASSIC in the optimizations, we evaluated GPP and ET simulated with CLASSIC using the optimized PFT-level V_{cmax25} against the same observations used for the optimizations. Please see our responses to **R1.C4** for further clarification.

In addition, we have added a statement to clarify this point.

Section 3.2, Paragraph 1 (Page 12, Lines 268–269):

"*The PFT-level V_{cmax25} was well constrained in the "single-site" and "all-site" optimizations, supporting the good quality of the optimizations using multi-year daily GPP and ET observations as the constraints (Fig. 4a).*"

(**R2.C3**) 2. The study does not include a sensitivity analysis of the parameters. And through the Farquhar equation, the relationship between GPP and Vcmax is easier to understand. Why choose ET to optimize Vcmax needs more explanation in model structure. To my knowledge, ET is sensitive to the parameters that control stomatal conductance change.

Our efforts in this study were aimed at refining a PFT-level V_{cmax25} parameterization in CLASSIC for North America's boreal forests using a Bayesian optimization framework. Please see our responses to **R1.C1** for our motivation.

In the "Farquhar" photosynthesis model implemented in CLASSIC, the PFT-level V_{cmax25} parametrization is of great importance in simulating ET by influencing the coupling between photosynthesis and canopy conductance. The optimizations using both GPP and ET observations were widely conducted in previous studies to optimize photosynthesis models (Groenendijk et al., 2011a; Groenendijk et al., 2011b; Santaren et al., 2007; Ueyama et al., 2016; He et al., 2014; Mo et al., 2008), including studies focusing on V_{cmax} optimization (Groenendijk et al., 2011b; Ueyama et al., 2016; He et al., 2014). Similarly, observed GPP and ET were used to jointly optimize PFT-level V_{cmax25} in CLASSIC in this study.

We have revised our statements to explain the CLASSIC model structure and the cost function used in the optimizations.

Section 2.1, Paragraph 1 (Page 4, Lines 105–111):

"*The CLASSIC model is the TBM in the Canadian suite of climate and Earth system models (Melton et al., 2020). Leaf-level photosynthesis is simulated using the "Farquhar" model commonly with a big-leaf parametrization (Melton and Arora, 2016; Arora, 2003; Farquhar et al., 1980). The simulated photosynthetic rate is jointly limited by the light, RuBisCO enzyme, and transport capacity.* V_{cmax} *is one of the key parameters to simulate limitations by the RuBisCO enzyme and transport capacity. The approach of Leuning (1995) is used for coupling photosynthesis and canopy conductance, and the latter is used to constrain water loss through transpiration.*"

Section 2.3, Paragraph 1 (Page 6, Lines 161–165):

"*To well constrain PFT-level* V_{cmax25} *in CLASSIC, we defined cost function based on GPP and ET (Groenendijk et al., 2011a; Ueyama et al., 2016; He et al., 2014). Specifically, the cost function was the normalized root mean square error (*$RMSE_n$*) of daily GPP (g C* m^{-2} day^{-1}*) and ET (mm* day^{-1}*) simulated with CLASSIC and corresponding daily observations obtained from eddy covariance measurements.*"

(**R2.C4**) 3. To avoid attributing all uncertainties of simulation results to Vcmax25, I suggest optimizing several key parameters of the carbon and water cycles together.

Our aims were to refine a PFT-level V_{cmax25} parameterization in CLASSIC, which might be a major contributor to the limited model skill in reproducing observed daily GPP and ET in boreal forest stands in North America based on our previous work (Qu et al., 2023). Please see our responses to **R1.C1** for our motivation. Optimizing other PFT-level parameters is beyond the scope of this study. Due to equifinality in model parameters, adding more PFT-level parameters to the optimizations would greatly increase the risk of poorly constrained optimizations, thus increasing the uncertainty in the results and reducing the applicability of optimized site-specific parameters to regional and global scales (Tang and Zhuang, 2008). We had discussed several possible sources of uncertainty in our optimized PFT-level V_{cmax25} associated with stand-level model representation of soils and plants and model parameterizations for photosynthesis and evapotranspiration in CLASSIC (please see section 3.5 in the manuscript).

In addition, our optimized PFT-level V_{cmax25} has been successfully used by other TBM modeling studies to improve regional simulations and to advance model development in CLASSIC (please see our responses to **R1.C1)**.

Minor comments

(R2.C5) 1. In section 2.2, a map of the distribution of the eight mature boreal forest stands is needed.

We have added a map showing forest stand locations in this study.

Section 2.2, Figure 1:

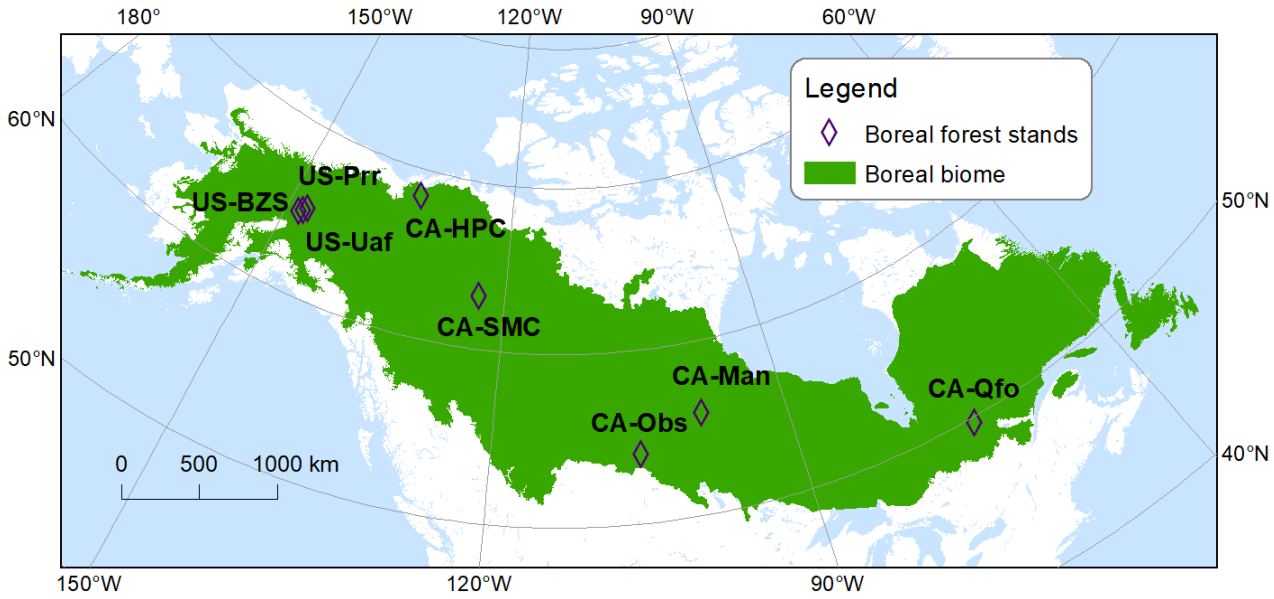

Figure 1. Forest stand locations across the boreal biome in North America (Brandt, 2009). Forest stand names refer to AmeriFlux IDs: CA-Qfo (Quebec - Eastern Boreal, Mature Black Spruce), CA-Obs (Saskatchewan - Western Boreal, Mature Black Spruce [in the former BOREAS Southern Study Area]), CA-Man (Manitoba - Northern Old Black Spruce [in the former BOREAS Northern Study Area]), CA-SMC (Smith Creek), US-BZS (Bonanza Creek Black Spruce), US-Uaf (University of Alaska, Fairbanks), US-Prr (Poker Flat Research Range Black Spruce Forest), and CA-HPC (Havikpak Creek). CA-Obs, CA-Qfo and CA-Man are permafrost-free forest stands, while CA-SMC, US-BZS, US-Uaf, and US-Prr are distributed in the discontinuous permafrost zone and CA-HPC is distributed in the continuous permafrost zone (Table S2).

(R2.C6) 2. How many site-years were used in optimization needs to be described in Table S2.

We have revised Table S2 to show the site-years used for the optimizations. Please see our responses to **R1.C3**.

(**R2.C7**) 3. Generally, in site optimization, the details of simulated results against observations before and after optimization should be shown as a series of figures on a daily time scale. These figures are important for audiences to understand the improvement of model performance.

Our model performance evaluation was in the daily time scale based on daily GPP and ET simulations with CLASSIC and daily observations obtained from eddy covariance measurements. Please see our responses to **R1.C4** for our clarifications and revisions.

To address this comment, we have added additional figures to show model performance in the daily time series against the same daily observations used for the optimizations. Accordingly, we have added our statements to analyze the additional figures.

Section 3.1, Paragraph 1 (Pages 9–10, Lines 235–243):

"Model performance improvement using the "single-site" optimized PFT-level V_{cmax25} was also found in the observed seasonality of daily GPP and ET in all forest stands (Fig. S3 and S4). Simulated daily GPP and ET using the "single-site" optimized PFT-level V_{cmax25} were significantly correlated with observed daily GPP (r = 0.79 to 0.94) and ET (r = 0.81 to 0.92). In addition, enhanced correlations between daily GPP simulations using the "single-site" optimized PFT-level V_{cmax25} and observations were found in most forest stands (Table S4)."

Supplementary materials, Figures S3 and S4:

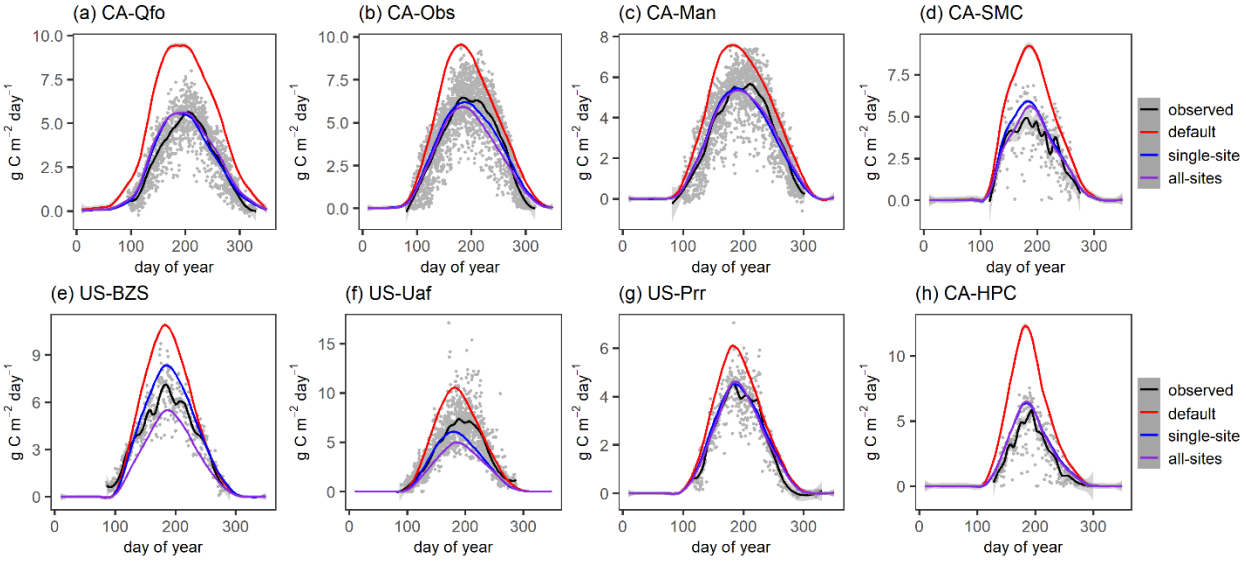

Figure S3. CLASSIC daily gross primary production (GPP) using the default and optimized plant functional type-level V_{cmax25} ("single-site" and "all-sites") compared with observations obtained from eddy covariance measurements over forest stands (a–h). Daily GPP is smoothed over the year using the locally estimated scatterplot smoothing with the moving-window width of 20 % of the data (Jacoby, 2000; Cleveland and Loader, 1996). For the "single-site" and "all-sites" optimizations the daily averages of iterative model simulations are used. Forest stand names refer to AmeriFlux IDs and forest stands are in a latitudinal order from south (CA-Qfo [a]) to north (CA-HPC [h]) (Fig. 1 and Table S2).

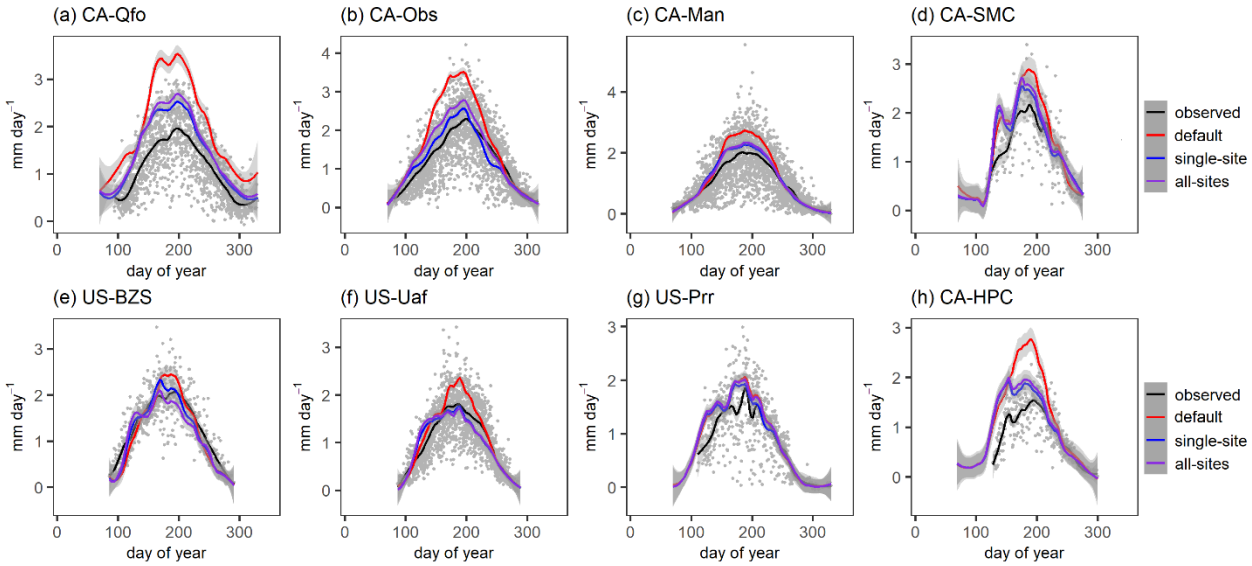

Figure S4. CLASSIC daily evapotranspiration (ET) using the default and optimized plant functional type-level V_{cmax25} ("single-site" and "all-sites") compared with observations obtained from eddy covariance measurements over forest stands (a–h). Daily ET is smoothed over the year using the locally estimated scatterplot smoothing with the moving-window width of 20 % of the data (Jacoby, 2000; Cleveland and Loader, 1996). For the "single-site" and "all-sites" optimizations the daily averages of iterative model simulations are used. Forest stand names refer to AmeriFlux IDs and forest stands are in a latitudinal order from south (CA-Qfo [a]) to north (CA-HPC [h]) (Fig. 1 and Table S2).

References

Ahmed, H. F., Helgason, W., Barr, A., and Black, A.: Characterization of spring thaw and its relationship with carbon uptake for different types of southern boreal forest, Agr. Forest Meteorol., 307, 108511, https://doi.org/10.1016/j.agrformet.2021.108511, 2021.

Ali, A. A., Xu, C., Rogers, A., McDowell, N. G., Medlyn, B. E., Fisher, R. A., Wullschleger, S. D., Reich, P. B., Vrugt, J. A., and Bauerle, W. L.: Global-scale environmental control of plant photosynthetic capacity, Ecol. Appl., 25, 2349-2365, https://doi.org/10.1890/14-2111.1, 2015.

Allison, S. D. and Treseder, K. K.: Climate change feedbacks to microbial decomposition in boreal soils, Fungal Ecol., 4, 362-374, https://doi.org/10.1016/j.funeco.2011.01.003, 2011.

Alton, P. B.: Retrieval of seasonal Rubisco-limited photosynthetic capacity at global FLUXNET sites from hyperspectral satellite remote sensing: Impact on carbon modelling, Agr. Forest Meteorol., 232, 74-88, https://doi.org/10.1016/j.agrformet.2016.08.001, 2017.

Arora, V. K.: Simulating energy and carbon fluxes over winter wheat using coupled land surface and terrestrial ecosystem models, Agr. Forest Meteorol., 118, 21-47, https://doi.org/10.1016/S0168-1923(03)00073-X, 2003.

Baltzer, J. L., Day, N. J., Walker, X. J., Greene, D., Mack, M. C., Alexander, H. D., Arseneault, D., Barnes, J., Bergeron, Y., and Boucher, Y.: Increasing fire and the decline of fire adapted black spruce in the boreal forest, PNAS, 118, e2024872118, https://doi.org/10.1073/pnas.2024872118, 2021.

Bauerle, W. L., Oren, R., Way, D. A., Qian, S. S., Stoy, P. C., Thornton, P. E., Bowden, J. D., Hoffman, F. M., and Reynolds, R. F.: Photoperiodic regulation of the seasonal pattern of photosynthetic capacity and the implications for carbon cycling, PNAS, 109, 8612-8617, https://doi.org/10.1073/pnas.1119131109, 2012.

Bergeron, O., Margolis, H. A., Black, T. A., Coursolle, C., Dunn, A. L., Barr, A. G., and Wofsy, S. C.: Comparison of carbon dioxide fluxes over three boreal black spruce forests in Canada, Glob. Change Biol., 13, 89-107, https://doi.org/10.1111/j.1365-2486.2006.01281.x, 2007.

Bergstra, J., Komer, B., Eliasmith, C., Yamins, D., and Cox, D. D.: Hyperopt: a python library for model selection and hyperparameter optimization, Comput. Sci. Discov., 8, 014008, https://doi.org/10.1088/1749-4699/8/1/014008, 2015.

Bergstra, J., Bardenet, R., Bengio, Y., and Kégl, B.: Algorithms for hyper-parameter optimization, in: Advances in Neural Information Processing Systems, Curran Associates, Inc., ISBN 9781618395993, 2011.

Bonan, G. B., Lawrence, P. J., Oleson, K. W., Levis, S., Jung, M., Reichstein, M., Lawrence, D. M., and Swenson, S. C.: Improving canopy processes in the Community Land Model version 4 (CLM4) using

global flux fields empirically inferred from FLUXNET data, J. Geophys. Res.-Biogeo., 116, G02014, https://doi.org/10.1029/2010JG001593, 2011.

Brandt, J. P.: The extent of the North American boreal zone, Environ. Rev., 17, 101-161, https://doi.org/10.1139/A09-004, 2009.

Breiman, L.: Random forests, Mach. Learn., 45, 5-32, https://doi.org/10.1023/A:1010933404324, 2001.

Cai, T. and Dang, Q.-L.: Effects of soil temperature on parameters of a coupled photosynthesis–stomatal conductance model, Tree Physiol., 22, 819-828, https://doi.org/10.1093/treephys/22.12.819, 2002.

Cleveland, W. S. and Loader, C.: Smoothing by local regression: Principles and methods, in: Statistical theory and computational aspects of smoothing, Springer, 10-49, 1996.

Croft, H., Chen, J. M., Luo, X., Bartlett, P., Chen, B., and Staebler, R. M.: Leaf chlorophyll content as a proxy for leaf photosynthetic capacity, Glob. Change Biol., 23, 3513-3524, https://doi.org/10.1111/gcb.13599, 2017.

Curasi, S. R., Melton, J. R., Humphreys, E. R., Wang, L., Seiler, C., Cannon, A. J., Chan, E., and Qu, B.: Evaluating the Performance of the Canadian Land Surface Scheme Including Biogeochemical Cycles (CLASSIC) Tailored to the Pan-Canadian Domain, J. Adv. Model. Earth Sy., 15, e2022MS003480, https://doi.org/10.1029/2022MS003480, 2023.

Detto, M. and Xu, X.: Optimal leaf life strategies determine Vc,max dynamic during ontogeny, New Phytol., 228, 361-375, https://doi.org/10.1111/nph.16712, 2020.

Dong, N., Prentice, I. C., Wright, I. J., Evans, B. J., Togashi, H. F., Caddy-Retalic, S., McInerney, F. A., Sparrow, B., Leitch, E., and Lowe, A. J.: Components of leaf-trait variation along environmental gradients, New Phytol., 228, 82-94, https://doi.org/10.1111/nph.16558, 2020.

Druel, A., Peylin, P., Krinner, G., Ciais, P., Viovy, N., Peregon, A., Bastrikov, V., Kosykh, N., and Mironycheva-Tokareva, N.: Towards a more detailed representation of high-latitude vegetation in the global land surface model ORCHIDEE (ORC-HL-VEGv1. 0), Geosci. Model Dev., 10, 4693-4722, https://doi.org/10.5194/gmd-10-4693-2017, 2017.

Dunn, A. L., Barford, C. C., Wofsy, S. C., Goulden, M. L., and Daube, B. C.: A long-term record of carbon exchange in a boreal black spruce forest: Means, responses to interannual variability, and decadal trends, Glob. Change Biol., 13, 577-590, https://doi.org/10.1111/j.1365-2486.2006.01221.x, 2007.

Dunne, J. P., Horowitz, L. W., Adcroft, A. J., Ginoux, P., Held, I. M., John, J. G., Krasting, J. P., Malyshev, S., Naik, V., Paulot, F., Shevliakova, E., Stock, C. A., Zadeh, N., Balaji, V., Blanton, C., Dunne, K. A., Dupuis, C., Durachta, J., Dussin, R., Gauthier, P. P. G., Griffies, S. M., Guo, H., Hallberg, R. W., Harrison, M., He, J., Hurlin, W., McHugh, C., Menzel, R., Milly, P. C. D., Nikonov, S., Paynter, D. J., Ploshay, J., Radhakrishnan, A., Rand, K., Reichl, B. G., Robinson, T., Schwarzkopf, D. M.,

Sentman, L. T., Underwood, S., Vahlenkamp, H., Winton, M., Wittenberg, A. T., Wyman, B., Zeng, Y., and Zhao, M.: The GFDL Earth System Model Version 4.1 (GFDL-ESM 4.1): Overall Coupled Model Description and Simulation Characteristics, J. Adv. Model. Earth Sy., 12, e2019MS002015, https://doi.org/10.1029/2019MS002015, 2020.

Ellison, A. M.: Bayesian inference in ecology, Ecol. Lett., 7, 509-520, https://doi.org/10.1111/j.1461-0248.2004.00603.x, 2004.

Euskirchen, E. S., Edgar, C., Turetsky, M., Waldrop, M. P., and Harden, J. W.: Differential response of carbon fluxes to climate in three peatland ecosystems that vary in the presence and stability of permafrost, J. Geophys. Res.-Biogeo., 119, 1576-1595, https://doi.org/10.1002/2014JG002683, 2014.

Evans, J. R. and Seemann, J. R.: The allocation of protein nitrogen in the photosynthetic apparatus: costs, consequences, and control, Photosynthesis, 8, 183-205, 1989.

Farquhar, G. D., von Caemmerer, S. v., and Berry, J. A.: A biochemical model of photosynthetic CO2 assimilation in leaves of C3 species, Planta, 149, 78-90, https://doi.org/10.1007/BF00386231, 1980.

Fisher, J. B., Hayes, D. J., Schwalm, C. R., Huntzinger, D. N., Stofferahn, E., Schaefer, K., Luo, Y., Wullschleger, S. D., Goetz, S., and Miller, C. E.: Missing pieces to modeling the Arctic-Boreal puzzle, Environ. Res. Lett., 13, 020202, https://doi.org/10.1088/1748-9326/aa9d9a, 2018.

Friend, A. D., Arneth, A., Kiang, N. Y., Lomas, M., Ogee, J., Rödenbeck, C., Running, S. W., SANTAREN, J. D., Sitch, S., and Viovy, N.: FLUXNET and modelling the global carbon cycle, Glob. Change Biol., 13, 610-633, https://doi.org/10.1111/j.1365-2486.2006.01223.x, 2007.

Gaumont-Guay, D., Black, T., Barr, A., Griffis, T., Jassal, R., Krishnan, P., Grant, N., and Nesic, Z.: Eight years of forest-floor CO2 exchange in a boreal black spruce forest: Spatial integration and long-term temporal trends, Agr. Forest Meteorol., 184, 25-35, https://doi.org/10.1016/j.agrformet.2013.08.010, 2014.

Gelbart, M. A., Snoek, J., and Adams, R. P.: Bayesian optimization with unknown constraints, arXiv [preprint], arXiv:1403.5607, https://doi.org/10.48550/arXiv.1403.5607, 2014.

Goldstein, A., Kapelner, A., Bleich, J., and Pitkin, E.: Peeking inside the black box: Visualizing statistical learning with plots of individual conditional expectation, J. Comput. Graph. Stat., 24, 44-65, https://doi.org/10.1080/10618600.2014.907095, 2015.

Groenendijk, M., Dolman, A., Van Der Molen, M., Leuning, R., Arneth, A., Delpierre, N., Gash, J., Lindroth, A., Richardson, A., and Verbeeck, H.: Assessing parameter variability in a photosynthesis model within and between plant functional types using global Fluxnet eddy covariance data, Agr. Forest Meteorol., 151, 22-38, https://doi.org/10.1016/j.agrformet.2010.08.013, 2011a.

Groenendijk, M., Dolman, A. J., Ammann, C., Arneth, A., Cescatti, A., Dragoni, D., Gash, J., Gianelle, D., Gioli, B., and Kiely, G.: Seasonal variation of photosynthetic model parameters and leaf area index

from global Fluxnet eddy covariance data, J. Geophys. Res.-Biogeo., 116, https://doi.org/10.1029/2011JG001742, 2011b.

He, L., Chen, J. M., Liu, J., Mo, G., Bélair, S., Zheng, T., Wang, R., Chen, B., Croft, H., and Arain, M. A.: Optimization of water uptake and photosynthetic parameters in an ecosystem model using tower flux data, Ecol. Model., 294, 94-104, https://doi.org/10.1016/j.ecolmodel.2014.09.019, 2014.

He, L., Chen, J. M., Liu, J., Zheng, T., Wang, R., Joiner, J., Chou, S., Chen, B., Liu, Y., and Liu, R.: Diverse photosynthetic capacity of global ecosystems mapped by satellite chlorophyll fluorescence measurements, Remote Sens. Environ., 232, 111344, https://doi.org/10.1016/j.rse.2019.111344, 2019.

Heijmans, M. M., Arp, W. J., and Chapin III, F. S.: Carbon dioxide and water vapour exchange from understory species in boreal forest, Agr. Forest Meteorol., 123, 135-147, https://doi.org/10.1016/j.agrformet.2003.12.006, 2004.

Helbig, M., Chasmer, L. E., Desai, A. R., Kljun, N., Quinton, W. L., and Sonnentag, O.: Direct and indirect climate change effects on carbon dioxide fluxes in a thawing boreal forest–wetland landscape, Glob. Change Biol., 23, 3231-3248, https://doi.org/10.1111/gcb.13638, 2017.

Hobeichi, S., Abramowitz, G., and Evans, J.: Conserving Land–Atmosphere Synthesis Suite (CLASS), J. Climate, 33, 1821-1844, https://doi.org/10.1175/JCLI-D-19-0036.1, 2020.

Ikawa, H., Nakai, T., Busey, R. C., Kim, Y., Kobayashi, H., Nagai, S., Ueyama, M., Saito, K., Nagano, H., and Suzuki, R.: Understory CO2, sensible heat, and latent heat fluxes in a black spruce forest in interior Alaska, Agr. Forest Meteorol., 214, 80-90, https://doi.org/10.1016/j.agrformet.2015.08.247, 2015.

Jacoby, W. G.: Loess:: a nonparametric, graphical tool for depicting relationships between variables, Electoral Studies, 19, 577-613, https://doi.org/10.1016/S0261-3794(99)00028-1, 2000.

Jasinski, B. L., Hewitt, R. E., Mauritz, M., Miller, S. N., Schuur, E. A. G., Taylor, M. A., Walker, X. J., and Mack, M. C.: Plant foliar nutrient response to active layer and water table depth in warming permafrost soils, J. Ecol., 110, 1201-1216, https://doi.org/10.1111/1365-2745.13864, 2022.

Kattge, J., Knorr, W., Raddatz, T., and Wirth, C.: Quantifying photosynthetic capacity and its relationship to leaf nitrogen content for global-scale terrestrial biosphere models, Glob. Change Biol., 15, 976-991, https://doi.org/10.1111/j.1365-2486.2008.01744.x, 2009.

Krishnan, P., Black, T. A., Barr, A. G., Grant, N. J., Gaumont-Guay, D., and Nesic, Z.: Factors controlling the interannual variability in the carbon balance of a southern boreal black spruce forest, J. Geophys. Res.-Atmos., 113, https://doi.org/10.1029/2007JD008965, 2008.

Kuppel, S., Peylin, P., Chevallier, F., Bacour, C., Maignan, F., and Richardson, A.: Constraining a global ecosystem model with multi-site eddy-covariance data, Biogeosciences, 9, 3757-3776, https://doi.org/10.5194/bg-9-3757-2012, 2012.

Kuppel, S., Peylin, P., Maignan, F., Chevallier, F., Kiely, G., Montagnani, L., and Cescatti, A.: Model–data fusion across ecosystems: from multisite optimizations to global simulations, Geosci. Model Dev., 7, 2581-2597, https://doi.org/10.5194/gmd-7-2581-2014, 2014.

Lawrence, D. M., Fisher, R. A., Koven, C. D., Oleson, K. W., Swenson, S. C., Bonan, G., Collier, N., Ghimire, B., van Kampenhout, L., and Kennedy, D.: The Community Land Model version 5: Description of new features, benchmarking, and impact of forcing uncertainty, J. Adv. Model. Earth Sy., 11, 4245-4287, https://doi.org/10.1029/2018MS001583, 2019.

Leuning, R.: A critical appraisal of a combined stomatal-photosynthesis model for C3 plants, Plant Cell Environ., 18, 339-355, https://doi.org/10.1111/j.1365-3040.1995.tb00370.x, 1995.

Li, B., Ryu, Y., Jiang, C., Dechant, B., Liu, J., and Yan, Y.: BESS v2.0: A Satellite-driven and Coupled-process Model for Quantifying Global Land-atmosphere Radiation, Energy and CO2 Fluxes since 1982, AGU Fall Meeting 2021, New Orleans, LA, 13-17 December 2021, B15D-1463, 2021.

Li, X. and Xiao, J.: A global, 0.05-degree product of solar-induced chlorophyll fluorescence derived from OCO-2, MODIS, and reanalysis data, Remote Sens., 11, 517, https://doi.org/10.3390/rs11050517, 2019.

Liang, S., Cheng, J., Jia, K., Jiang, B., Liu, Q., Xiao, Z., Yao, Y., Yuan, W., Zhang, X., and Zhao, X.: The global land surface satellite (GLASS) product suite, B. Am. Meteorol. Soc., 102, E323-E337, https://doi.org/10.1175/BAMS-D-18-0341.1, 2021.

Liang, X., Zhang, T., Lu, X., Ellsworth, D. S., BassiriRad, H., You, C., Wang, D., He, P., Deng, Q., and Liu, H.: Global response patterns of plant photosynthesis to nitrogen addition: A meta-analysis, Glob. Change Biol., 26, 3585-3600, https://doi.org/10.1111/gcb.15071, 2020.

Maire, V., Wright, I. J., Prentice, I. C., Batjes, N. H., Bhaskar, R., van Bodegom, P. M., Cornwell, W. K., Ellsworth, D., Niinemets, Ü., and Ordonez, A.: Global effects of soil and climate on leaf photosynthetic traits and rates, Global Ecol. Biogeogr., 24, 706-717, https://doi.org/10.1111/geb.12296, 2015.

Martin, M. R., Kumar, P., Sonnentag, O., and Marsh, P.: Thermodynamic basis for the demarcation of Arctic and alpine treelines, Sci. Rep.-UK, 12, 1-14, https://doi.org/10.1038/s41598-022-16462-2, 2022.

Melton, J. R. and Arora, V. K.: Competition between plant functional types in the Canadian Terrestrial Ecosystem Model (CTEM) v.2.0, Geosci. Model Dev., 9, 323-361, https://doi.org/10.5194/gmd-9-323-2016, 2016.

Melton, J. R., Arora, V. K., Wisernig-Cojoc, E., Seiler, C., Fortier, M., Chan, E., and Teckentrup, L.: CLASSIC v1.0: the open-source community successor to the Canadian Land Surface Scheme (CLASS) and the Canadian Terrestrial Ecosystem Model (CTEM)–Part 1: Model framework and site-level performance, Geosci. Model Dev., 13, 2825-2850, https://doi.org/10.5194/gmd-13-2825-2020, 2020.

Mo, X., Chen, J. M., Ju, W., and Black, T. A.: Optimization of ecosystem model parameters through assimilating eddy covariance flux data with an ensemble Kalman filter, Ecol. Model., 217, 157-173, https://doi.org/10.1016/j.ecolmodel.2008.06.021, 2008.

Musavi, T., Migliavacca, M., van de Weg, M. J., Kattge, J., Wohlfahrt, G., van Bodegom, P. M., Reichstein, M., Bahn, M., Carrara, A., and Domingues, T. F.: Potential and limitations of inferring ecosystem photosynthetic capacity from leaf functional traits, Ecol. Evol., 6, 7352-7366, https://doi.org/10.1002/ece3.2479, 2016.

Nimalan, M., Ziyu, W., Firas, H., and Nando De, F.: Adaptive MCMC with Bayesian Optimization, Proceedings of the Fifteenth International Conference on Artificial Intelligence and Statistics, Chia Laguna Resort, Sardinia, Italy, 2012/03/21, http://proceedings.mlr.press/v22/mahendran12.html, 2012.

Pedregosa, F., Varoquaux, G., Gramfort, A., Michel, V., Thirion, B., Grisel, O., Blondel, M., Prettenhofer, P., Weiss, R., and Dubourg, V.: Scikit-learn: Machine learning in Python, J. Mach. Learn. Res., 12, 2825-2830, https://jmlr.csail.mit.edu/papers/v12/pedregosa11a.html, 2011.

Price, D. T., Alfaro, R., Brown, K., Flannigan, M., Fleming, R. A., Hogg, E., Girardin, M., Lakusta, T., Johnston, M., and McKenney, D.: Anticipating the consequences of climate change for Canada's boreal forest ecosystems, Environ. Rev., 21, 322-365, https://doi.org/10.1139/er-2013-0042, 2013.

Qu, B., Roy, A., Melton, J. R., Black, T. A., Amiro, B., Euskirchen, E. S., Ueyama, M., Kobayashi, H., Schulze, C., and Gosselin, G. H.: A boreal forest model benchmarking dataset for North America: a case study with the Canadian Land Surface Scheme Including Biogeochemical Cycles (CLASSIC), Environ. Res. Lett., 18, 085002, https://doi.org/10.1088/1748-9326/ace376 2023.

Rayment, M., Loustau, D., and Jarvis, P.: Photosynthesis and respiration of black spruce at three organizational scales: shoot, branch and canopy, Tree Physiol., 22, 219-229, https://doi.org/10.1093/treephys/22.4.219, 2002.

Reich, P. B., Sendall, K. M., Stefanski, A., Rich, R. L., Hobbie, S. E., and Montgomery, R. A.: Effects of climate warming on photosynthesis in boreal tree species depend on soil moisture, Nature, 562, 263-267, https://doi.org/10.1038/s41586-018-0582-4, 2018.

Rogers, A.: The use and misuse of Vc,max in Earth System Models, Photosynth. Res., 119, 15-29, https://doi.org/10.1007/s11120-013-9818-1, 2014.

Rogers, A., Serbin, S. P., Ely, K. S., Sloan, V. L., and Wullschleger, S. D.: Terrestrial biosphere models underestimate photosynthetic capacity and CO2 assimilation in the Arctic, New Phytol., 216, 1090-1103, https://doi.org/10.1111/nph.14740, 2017.

Rogers, A., Serbin, S. P., and Way, D. A.: Reducing model uncertainty of climate change impacts on high latitude carbon assimilation, Glob. Change Biol., 28, 1222– 1247, https://doi.org/10.1111/gcb.15958, 2021.

Running, S. and Zhao, M.: MOD17A2HGF MODIS/Terra Gross Primary Productivity Gap-Filled 8-Day L4 Global 500 m SIN Grid V061, NASA EOSDIS Land Processes DAAC [data set], https://doi.org/10.5067/MODIS/MOD17A2HGF.061, 2021.

Sahlin, K.: Estimating convergence of Markov chain Monte Carlo simulations, Master Thesis, Mathematical Statistics, Stockholm University, Sweden, 2011.

Salmon, V. G., Soucy, P., Mauritz, M., Celis, G., Natali, S. M., Mack, M. C., and Schuur, E. A. G.: Nitrogen availability increases in a tundra ecosystem during five years of experimental permafrost thaw, Glob. Change Biol., 22, 1927-1941, https://doi.org/10.1111/gcb.13204, 2016.

Santaren, D., Peylin, P., Viovy, N., and Ciais, P.: Optimizing a process-based ecosystem model with eddy-covariance flux measurements: A pine forest in southern France, Global Biogeochem. Cy., 21, GB2013, https://doi.org/10.1029/2006GB002834, 2007.

Schratz, P., Muenchow, J., Iturritxa, E., Richter, J., and Brenning, A.: Hyperparameter tuning and performance assessment of statistical and machine-learning algorithms using spatial data, Ecol. Model, 406, 109-120, https://doi.org/10.1016/j.ecolmodel.2019.06.002, 2019.

Schwalm, C. R., Williams, C. A., Schaefer, K., Anderson, R., Arain, M. A., Baker, I., Barr, A., Black, T. A., Chen, G., and Chen, J. M.: A model-data intercomparison of CO2 exchange across North America: Results from the North American Carbon Program site synthesis, J. Geophys. Res.-Biogeo., 115, G00H05, https://doi.org/10.1029/2009JG001229, 2010.

Slevin, D., Tett, S. F. B., Exbrayat, J. F., Bloom, A. A., and Williams, M.: Global evaluation of gross primary productivity in the JULES land surface model v3.4.1, Geosci. Model Dev., 10, 2651-2670, https://doi.org/10.5194/gmd-10-2651-2017, 2017.

Smith, N. G., Keenan, T. F., Colin Prentice, I., Wang, H., Wright, I. J., Niinemets, Ü., Crous, K. Y., Domingues, T. F., Guerrieri, R., and Yoko Ishida, F.: Global photosynthetic capacity is optimized to the environment, Ecol. Lett., 22, 506-517, https://doi.org/10.1111/ele.13210, 2019.

Stinziano, J. R., Bauerle, W. L., and Way, D. A.: Modelled net carbon gain responses to climate change in boreal trees: Impacts of photosynthetic parameter selection and acclimation, Glob. Change Biol., 25, 1445-1465, https://doi.org/10.1111/gcb.14530, 2019.

Strobl, C., Boulesteix, A.-L., Zeileis, A., and Hothorn, T.: Bias in random forest variable importance measures: Illustrations, sources and a solution, BMC bioinformatics, 8, 25, https://doi.org/10.1186/1471-2105-8-25, 2007.

Tang, J. and Zhuang, Q.: Equifinality in parameterization of process-based biogeochemistry models: A significant uncertainty source to the estimation of regional carbon dynamics, J. Geophys. Res.-Biogeo., 113, https://doi.org/10.1029/2008JG000757, 2008.

Tonteri, T., Salemaa, M., Rautio, P., Hallikainen, V., Korpela, L., and Merilä, P.: Forest management regulates temporal change in the cover of boreal plant species, Forest Ecol. Manag., 381, 115-124, https://doi.org/10.1016/j.foreco.2016.09.015, 2016.

Tramontana, G., Jung, M., Schwalm, C. R., Ichii, K., Camps-Valls, G., Ráduly, B., Reichstein, M., Arain, M. A., Cescatti, A., and Kiely, G.: Predicting carbon dioxide and energy fluxes across global FLUXNET sites with regression algorithms, Biogeosciences, 13, 4291-4313, https://doi.org/10.5194/bg-13-4291-2016, 2016.

Ueyama, M., Iwata, H., and Harazono, Y.: Autumn warming reduces the CO2 sink of a black spruce forest in interior Alaska based on a nine-year eddy covariance measurement, Glob. Change Biol., 20, 1161-1173, https://doi.org/10.1111/gcb.12434, 2014.

Ueyama, M., Tahara, N., Iwata, H., Euskirchen, E. S., Ikawa, H., Kobayashi, H., Nagano, H., Nakai, T., and Harazono, Y.: Optimization of a biochemical model with eddy covariance measurements in black spruce forests of Alaska for estimating CO2 fertilization effects, Agr. Forest Meteorol., 222, 98-111, https://doi.org/10.1016/j.agrformet.2016.03.007, 2016.

Verheijen, L., Brovkin, V., Aerts, R., Bönisch, G., Cornelissen, J., Kattge, J., Reich, P. B., Wright, I. J., and Van Bodegom, P.: Impacts of trait variation through observed trait–climate relationships on performance of an Earth system model: a conceptual analysis, Biogeosciences, 10, 5497-5515, https://doi.org/10.5194/bg-10-5497-2013, 2013.

Wullschleger, S. D., Epstein, H. E., Box, E. O., Euskirchen, E. S., Goswami, S., Iversen, C. M., Kattge, J., Norby, R. J., van Bodegom, P. M., and Xu, X.: Plant functional types in Earth system models: past experiences and future directions for application of dynamic vegetation models in high-latitude ecosystems, Ann. Bot.-London, 114, 1-16, https://doi.org/10.1093/aob/mcu077, 2014.

Xiao, J., Davis, K. J., Urban, N. M., and Keller, K.: Uncertainty in model parameters and regional carbon fluxes: A model-data fusion approach, Agr. Forest Meteorol., 189, 175-186, https://doi.org/10.1016/j.agrformet.2014.01.022, 2014.

Yan, Z., Sardans, J., Peñuelas, J., Detto, M., Smith, N. G., Wang, H., Guo, L., Hughes, A. C., Guo, Z., Lee, C. K. F., Liu, L., and Wu, J.: Global patterns and drivers of leaf photosynthetic capacity: The relative importance of environmental factors and evolutionary history, Global Ecol. Biogeogr., 32, 668-682, https://doi.org/10.1111/geb.13660, 2023.

Zhang, Y., Xiao, X., Wu, X., Zhou, S., Zhang, G., Qin, Y., and Dong, J.: A global moderate resolution dataset of gross primary production of vegetation for 2000–2016, Sci. Data, 4, 170165, https://doi.org/10.1038/sdata.2017.165, 2017.